Molecular Basis of Antimony Treatment in Leishmaniasis†

Paola Baiocco,‡ Gianni Colotti,‡,* Stefano Franceschini, and Andrea Ilari*

Istituto di Biologia e Patologia Molecolari—CNR and Department of Biochemical Sciences, Sapienza University of Roma, P.le A. Moro 5, 00185 Roma, Italy

Received February 13, 2009

Leishmaniasis is a disease that affects 2 million people and kills 70000 persons every year. It is caused by *Leishmania* species, which are human protozoan parasites of the trypanosomatidae family. Trypanosomatidae differ from the other eukaryotes in their specific redox metabolism because the glutathione/glutathione reductase system is replaced by the unique trypanothione/trypanothione reductase system. The current treatment of leishmaniasis relies mainly on antimonial drugs. The crystal structures of oxidized trypanothione reductase (TR) from *Leishmania infantum* and of the complex of reduced TR with NADPH and Sb(III), reported in this paper, disclose for the first time the molecular mechanism of action of antimonial drugs against the parasite. Sb(III), which is coordinated by the two redox-active catalytic cysteine residues (Cys52 and Cys57), one threonine residue (Thr335), and His461′ of the 2-fold symmetry related subunit in the dimer, strongly inhibits TR activity. Because TR is essential for the parasite survival and virulence and it is absent in mammalian cells, these findings provide insights toward the design of new more affordable and less toxic drugs against Leishmaniasis.

Introduction

Leishmaniasis is a poverty-related disease characterized by high morbidity, which is deeply linked to malnutrition, humanitarian emergencies, and environmental changes that affect vector biology. It causes an estimated 70000 deaths annually, a rate surpassed among parasitic diseases only by malaria.[1] This disease is transmitted by the bite of the sand fly of the genus *Leishmania* in the New World and of the fly of the genus *Phlebotomus* in the Old World. Usually, the parasite primarily infects a feral or domestic mammalian host. Most forms of the diseases are zoonotic, i.e., transmissible only among animals, but human leishmaniasis is increasingly spreading throughout the world. Human infection is caused by about 21 out of the 30 species that infect mammals. These include the *Leishmania donovani* complex with two main species (*L. donovani* and *Leishmania infantum*), the *Leishmania mexicana* complex with three main species (*L. mexicana, Leishmania amazonensis*, and *Leishmania venezuelensis*), *Leishmania tropica*, *Leishmania major*, *Leishmania aethiopica*, and the subgenus *Viannia* with four main species (*Leishmania (V.) braziliensis, Leishmania (V.) guyanensis, Leishmania (V.) panamensis*, and *Leishmania (V.) peruviana*).[2−5] Leishmania parasites are widespread in 22 countries in the New World and in 66 nations in the Old World. Endemic regions have been spreading increasingly over the last ten years, with a sharp increase in the number of recorded cases. Indeed, 2 million new cases are considered to occur annually, with an estimated 12 million people presently infected worldwide. Leishmaniasis comprises two major clinical forms, visceral leishmaniasis, caused by *L. donovani* and *L. infantum*, which is invariably fatal, if untreated, and the cutaneous form, which can heal spontaneously but leaves disfiguring scars.[5]

The current treatment of leishmaniasis relies on antimony-based drugs, meglumine antimoniate (Glucantime), and sodium stibogluconate (Pentostam). However, the molecular mechanism of action of these drugs is not completely understood and their use is severely impaired by the side effects related to their toxicity. In addition, an ever increasing number of drug-resistant strains have been identified in Bihar, India, which prevents the use of antimonial drugs in this endemic area.[6−8] Therefore, on the one hand, there is an urgent need to develop novel drugs that target specific metabolic pathways of the parasite; on the other hand, it is also necessary to understand the mechanism of action of the most used drugs in order to minimize their severe side effects.

The recent completion of the *L. major*, *L. infantum*, and *L. brasiliensis* genome sequencing projects provided researchers worldwide with a wealth of information, enabling them to study the parasite metabolism and detect new molecular targets for pharmaceutical treatment. Among the potential molecular targets to date, trypanothione synthetase (TS[a]) and trypanothione reductase (TR), the putative enzyme targeted by antimonial compounds, are most promising in that they are involved in the unique thiol-based metabolism of *Leishmania*, which is common to all parasites of the Trypanosomatidae family but absent in the host. TS synthesizes a glutathione−spermidine conjugate named trypanothione (N1−N8-bis(glutathionyl)spermidine), and TR keeps this molecule reduced.[9−11] The trypanothione/TR system replaces many of the antioxidant and metabolic functions of the glutathione/glutathione reductase (GR) and thioredoxin/thioredoxin reductase systems present in other organisms and, for this reason, it is necessary for the protozoa survival.[12−16]

Pentavalent antimonials, which are the first choice drugs for the treatment of visceral leishmaniasis, are known to be active

† Atomic coordinates and structure factors have been deposited in the Protein Data Bank (www.ebi.ac.uk/msd). PDB accession codes: 2JK6 for oxidized TR and 2W0H for reduced TR in complex with NADPH and Sb(III).

* To whom correspondence should be addressed. Phone: 0039-06-49910910. Fax: 0039-06-4440062. E-mail: Gianni.colotti@uniroma1.it (G.C.); Andrea.ilari@uniroma1.it (A.I.).

‡ These two authors contributed equally to the work.

[a] Abbreviations: TS, trypanothione synthetase; TR, trypanothione reductase; GR, glutathione reductase; NADPH, nicotinamide adenine dinucleotide phosphate; Tris, tris(hydroxymethyl)-aminomethane/HCl; FAD, flavin adenine dinucleotide; TS_2, oxidized trypanothione; Hepes, 4-(2-hydroxyethyl)-1-piperazineethanesulfonic acid; ROS, reactive oxygen species; $T(SH)_2$, reduced trypanothione.

10.1021/jm900185q CCC: $40.75
Published on Web 03/24/2009

only following bioreduction to the trivalent Sb(III) form. Fairlamb and co-workers discovered that trivalent antimonials inhibit TR and that reduction of TR by nicotinamide adenine dinucleotide phosphate (NADPH) is essential for inhibition. In vivo, antimonials interfere with trypanothione metabolism by inducing rapid efflux of intracellular trypanothione and glutathione and inhibiting TR in intact cells. Despite these findings, the molecular basis of the interaction of antimonials with TR and of its inhibition is still unknown.[17−19]

In this paper, the crystal structures of TR from *Leishmania infantum* in the oxidized state and of the complex of TR with NADPH and Sb(III) in the reduced state (the first TR structures from *Leishmania* species) are presented.

Comparison between the two structures allowed us to identify the structural elements involved in NADPH and Sb(III) binding to TR. Additionally, the discovery of the structural differences between the oxidized enzyme in the free state and the bound reduced enzyme provides further elements to understand the mechanism of trypanothione reduction. Most importantly, the structural analysis of TR in complex with NADPH and Sb(III) permitted the identification of the Sb(III) binding site. This, together with the enzymatic activity experiments, discloses for the first time the molecular basis of TR inhibition by antimonials. The knowledge of the mechanism of action of the antimonial drugs at the molecular level provides essential information to rationally design new, less toxic, and more affordable drugs aimed at TR inhibition.

Interestingly, the only other protein structure containing Sb(III) reported to date is the crystal structure of the catalytic subunit of *E. coli* ArsA ATPase (PDB code, 1F48).[20] Hence, the structure of the Sb(III)−*L. infantum* TR complex furnishes important structural information on the coordination geometry of Sb(III) in proteins.

Experimental Section

Crystallization. Cloning, expression, and purification of TR from *Leishmania infantum* were carried out as previously reported.[21] Crystallization trials of TR from *L. infantum* were initially performed by sitting drop robotized screening at 293 K using several commercially available crystallization kits (Wizard screen, Emerald Biosystems; Index screen and Crystal screen, Hampton Research). Crystallization trials were performed using a protein sample concentrated to about 8 mg/mL and dialyzed against 20 mM tris(hydroxymethyl)-aminomethane/HCl (Tris), pH = 7.5. Aliquots of 0.1 μL of protein sample were mixed by the crystallization robot with an equal amount of the reservoir solution. Small crystals grew after two weeks in the trial 4 of the Crystal Screen I (Hampton Research), containing the crystallization solution: 0.1 M Tris pH = 8.5, 2.0 M ammonium sulfate.

Crystals were optimized by hand using the hanging drop vapor diffusion method. The measured crystal was obtained using ammonium sulfate as precipitant agent in a final concentration of 2.2 M and Tris buffer at a pH 8.5 in a final concentration of 0.1 M. One μL aliquots of the protein sample were mixed with an equal amount of the reservoir solution and allowed to equilibrate with a 500 μL volume of reservoir solution. The crystals grew at a controlled temperature of 294 K, reaching dimensions of 0.3 mm × 0.3 mm × 0.2 mm in 10−15 days.

Crystals of TR complexed with NADPH and Sb(III) were obtained by soaking crystals of free oxidized TR for two hours with a stabilizing solution of 2.5 M ammonium sulfate, 0.1 M Tris at pH 8.5, containing 1 mM potassium antimonyl tartrate trihydrate and 5 mM NADPH (Sigma Aldrich).

All TR crystals were cryoprotected in a solution containing 75% v/v of the reservoir solution and 25% v/v of glycerol and mounted in nylon loops. Then, the crystals were flash-frozen by quick submersion into liquid nitrogen for transport to a synchrotron radiation source.

Table 1. Crystal Parameters, Data Collection, and Refinement Statistics[a]

	oxidized TR	reduced TR + NADPH + Sb(III)
Data Collection		
space group	*P*41	*P*41
unit cell dimensions (Å)	103.45, 103.45, 192.62	102.99, 102.99, 193.18
resolution range (Å)	49−2.95 (3.0−2.95)	48−3.0 (3.08−3.0)
total reflections (unique reflections)	199626 (41850)	199810 (44389)
completeness (%)	98.6 (84.1)	99.9 (99.8)
R_{merge}	0.055 (0.295)	0.111 (0.365)
redundancy	4.8 (3.4)	4.5 (4.5)
$\langle I/\sigma(I)\rangle$	23.1 (3.8)	9.6 (3.6)
Refinement Statistics		
resolution range (Å)	40.0−2.95 (3.0−2.95)	40−3.0 (3.08−3.00)
number of reflections	39182 (2576)	33190 (2431)
free *R* value	0.264 (0.360)	0.261 (0.365)
R value (working set)	0.235 (0.308)	0.237 (0.371)
rmsd of bond lengths (Å)	0.006	0.006
rmsd of angles (deg)	0.944	1.102
FAD	2	2
NADPH		2
antimony		2
waters	16	26
sulfate ions	5	2
Ramachandran Analysis		
residues in most favored regions (%)	96.8	93.8
residues in additionally allowed regions (%)	3.2	6.2
outliers	0	0

[a] Values in parentheses are for the highest resolution shell.

Data Collection and Data Reduction. Single wavelength data sets (λ = 0.91841 Å) were collected from crystals of oxidized TR and of reduced TR in complex with NADPH and Sb(III) on the BL 14-2 beamline at the Synchrotron Radiation Source BESSY, Berlin, Germany, using a CCD detector at a temperature of 100 K.

The autoindexing procedure performed with DENZO[22] indicated that the crystals were tetragonal. The data scaling, performed with SCALEPACK,[22] indicated that the crystals belong to the $P4_1$ space group. Crystal parameters and data collection statistics for the measured diffracting crystal are given in Table 1.

Assuming a molecular weight of about 54 kDa per monomer, the presence of four asymmetric units in the $P4_1$ cell and of two molecules in the asymmetric unit, the value of V_M appears to be very high (4.67 Å^3 Da^{-1}), with a very high solvent content (74%).[21] This fact is unusual but not unprecedented and is consistent with the fact that despite their regular shape and big dimensions the TR crystals do not diffract better than 2.95 Å.

Structures Solution, Model Building, and Refinement. Native Oxidized TR. The structure of native oxidized *L. infantum* TR was solved by molecular replacement using as search model the TR from *Crithidia fasciculata* (PDB code 1FEA), which has sequence identity of 78% with *L. infantum* TR. The rotational and translational searches, performed with the program MolRep[23] (CCP4 suite) in the resolution range of 10−3.5 Å, produced a clear solution, corresponding to a dimer in the asymmetric unit.

Refinement was performed using the maximum likelihood method with the program REFMAC5[24] and model building was carried out using the program COOT[25] (see Table 1). The final model of native TR is a dimer that contains 978 residues (489 for each monomer), two FAD molecules, 16 water molecules, and five sulfate anions. The final R_{crys} for all resolution shells (40−2.95 Å) calculated using the working set reflections (39182) is 23.5%, and the Free *R* value calculated using the test set reflections (2057) is 26.4%. The final R_{crys} calculated for the highest resolution shell

(3.0−2.95 Å) using the working set reflections (2576) is 30.8%, and the Free *R* value calculated using the test set of reflections (162) is 36.0%. The most favored regions of the Ramachandran plot contain 96.8% of nonglycine residues. The atomic coordinates and structure factors have been deposited in the Protein Data Bank (PDB accession code for native TR: 2JK6).

Complex of Reduced TR with NADPH and Sb(III). Because the cell dimensions of TR in complex with NADPH and Sb(III) are slightly different from the native oxidized TR (see Table 1), we used molecular replacement to correctly position the protein in the new cell. The rotational and translational searches were performed with the program MolRep[23] using as search model the native TR structure in the resolution range of 10−3.5 Å and produced a clear solution.

Refinement and model building were performed as described above for the native oxidized TR. The final model of TR in complex with NADPH and Sb(III) is a dimer that contains 972 residues (485 for the monomer A and 487 for the monomer B), 26 water molecules, two sulfate anions, two flavin adenine dinucleotide (FAD) molecules, two NADPH molecules, and two Sb(III) (one metal ion per monomer). The final R_{crys} for all resolution shells (40.0−3.0 Å) calculated using the working set reflections (33190) is 23.8%, and the free *R* value, calculated using the test set reflections (1788), is 26.1%. The final R_{crys} calculated for the highest resolution shell (3.08−3.00 Å) using the working set reflections (2431) is 36.5% and the Free *R* value calculated using the test set reflections (131) is 37.1%. The most favored regions of the Ramachandran plot contain 93.8% of non-glycine residues. The atomic coordinates and structure factors have been deposited in the Protein Data Bank. The PDB accession code for TR in complex with NADPH and Sb(III) is 2W0H.

TR Assay and Inhibition. TR activity was measured at 25 °C in a diode array Hewlett-Packard HP8452A spectrophotometer. The standard assay (0.8 mL) contained NADPH, oxidized trypanothione (TS_2), and 20 nM TR in TR assay buffer: 40 mM 4-(2-hydroxyethyl)-1-piperazineethanesulfonic acid (Hepes), 50 mM NaCl, pH 7.5. NADPH was added to TR solution and incubated at 25 °C for 1 min immediately prior to addition of TS_2. Addition of TS_2 corresponds to time 0. After starting the reaction by addition of TS_2, the absorbance decrease at 340 nm was followed.

One U activity is defined as the amount of enzyme required to convert 1 pmol NADPH to $NADP^+$/min at 25 °C. The experiments for calculation of the K_m of TS_2 were carried out varying TS_2 concentration, while NADPH concentration was 200 μM; experiments for calculation of the K_m of NADPH were carried out by varying NADPH concentration, while TS_2 concentration was 200 μM.

Experiments for calculation of the K_i of Sb(III) and As(III) were carried out by varying Sb(III) and As(III) concentration, while TS_2 and NADPH concentrations were 200 μM each. Oxidized trypanothione (Bachem), NADPH (Sigma), potassium antimonyl tartrate trihydrate (Sigma), and arsenic(III) oxide (Sigma) were used for the experiments.

Size-Exclusion Chromatography. Gel filtration experiments were carried out on a GE Healthcare Superose 6 10/300 column (manufacturers' exclusion limit 4×10^7 Da for proteins) using an Amersham Biosciences P-900 system. Highly purified TR was equilibrated by dialysis vs 100 mM Hepes buffer, pH 7.8, 150 mM sodium chloride. Then 0.5 mL samples were injected on the column equilibrated with 100 mM Hepes buffer, pH 7.8, 150 mM sodium chloride (flow rate 0.5 mL/min, detection 280 nm). Three different molecular weight standards (Dps particles, Amersham low molecular weight gel filtration kit 17-0442-01, Bio-Rad gel filtration standard 151-1901) were used to obtain a precise calibration curve.

Results

Spectroscopic Features of TR. TR from *L. infantum* possesses spectroscopic properties closely resembling those of other TRs.[19] The oxidized enzyme, where the redox-active cysteine residues Cys52 and Cys57 of the disulfide binding site are covalently linked by a disulfide bridge, exhibits absorbance maxima at 377 and 462 nm.

Addition of 200 μM NADPH as a reducing agent leads to a decrease of the absorbance at 462 nm with concomitant acquisition of a broad band (530 nm) due to reduction of the cysteine disulfide bridge and formation of a characteristic charge-transfer complex between the FAD and the proximal sulfhydryl group.

Structures Solution and Overall Fold. The crystal structure of *L. infantum* TR in its oxidized state has been solved at 2.95 Å resolution. All the TR crystals are well shaped but contain a high amount of solvent (solvent content = 74%)[26] and for this reason do not diffract better than 2.95 Å. The asymmetric unit contains a dimer formed by two identical subunits (rmsd = 0.02 Å), related by a 2-fold axis.

The overall fold of *L. infantum* TR closely resembles that of *C. fasciculata* TR and *Trypanosoma cruzi* TR (the superposition between the Cα atoms of *L. infantum* with *C. fasciculata* (PDB code 1FEA) and *T. cruzi* (PDB code 1BZL) TRs results in rmsd values of 0.62 and 0.87 Å, respectively) (Figure 1). Each monomer is formed by three different domains: the FAD binding domain (residues 1−160 and 289−360), the NADPH binding domain (residues 161−289) and the interface domain (361−488) (Figure 2), as described by Zhang et al.[27]

Dimeric Interface. As mentioned above, the asymmetric unit of both oxidized TR and reduced TR in complex with NADPH and Sb(III) contain dimers. Additionally, like GRs, TRs are known to be active in the dimeric state.[19] Experiments of size exclusion chromatography were carried out to determine whether *L. infantum* TR is dimeric in solution. The analysis of the elution pattern (not shown) demonstrates that the *L. infantum* TR used for crystallization experiments and enzymatic activity assays (see below) has a molecular weight of 105 ± 8 kDa, corresponding to a dimer (Table 2).

The dimeric interface, analyzed with ProtorP,[28] displays a large, solvent accessible, mostly nonpolar surface area of 3187.61 $Å^2$. In particular, the interface contains a 30.12% of polar residues, 53.01% of nonpolar residues, and 16.87% of charged residues. The residues involved in hydrogen bonds (distances between 2.52 Å and 3.15 Å) that stabilize the interface are: Lys61, Gly66, Phe79, Gly80, Trp81, Asn91, Tyr210, Glu436, Gln439, Ser440, Val460, Pro462, Ser464, and Ala465. Some of these interactions are conserved in human GR, but others are present only in *L. infantum* TR, namely: residues in the loop between the two longest helices in the FAD binding domain (Phe79, Gly80, Trp81, Asn91), Tyr210 in the NADPH binding domain, and Ser440 in the interface domain. Similarly to human GR and other members of TR family, in *L. infantum* TR, the dimeric interface contains two symmetric catalytic clefts where reduction of the trypanothione disulfide bridge takes place. Each cleft is formed by: the N-terminal part of helix 48−87, helices 16−25 and 334−348 of the FAD binding domain of one monomer, and loops 433−454 and 395−398 of the interface domain of the 2-fold symmetry-related monomer (Figure 2).

The FAD-Binding Domain. The FAD binding domain adopts the Rossmann fold typical of GR family members. It is formed by a three-stranded antiparallel β-sheet (residues 126−153), a five-stranded parallel β-sheet (strands 7−10, 31−35, 120−124, 155−158), and four α-helices (14−27, 24−92, 69−161, 335−351) (Figure 3A). Like the other TRs whose structures have been solved so far, *L. infantum* TR displays an active site larger than that of GRs.[27,29−32]

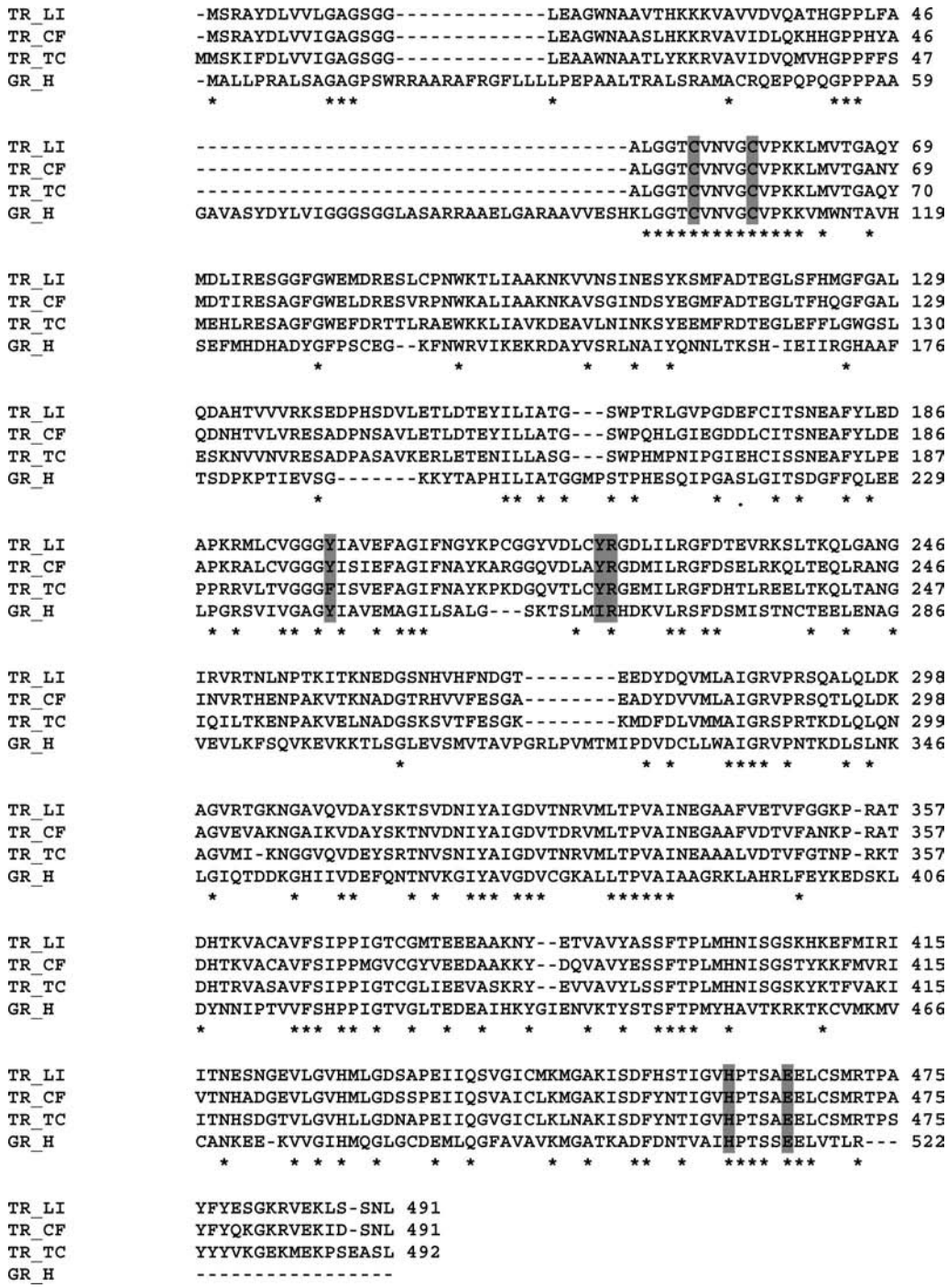

Figure 1. ClustalW[56]-generated multiple sequence alignment of *L. infantum* TR with *C. fasciculata* TR, *T. cruzi* TR, and human GR. Residues conserved in all sequences are indicated by asterisks. Residues involved in catalysis have gray background.

Almost all the residues interacting with FAD are conserved among the TR family member, although it is possible to observe some small differences. In *L. infantum* TR, N of Gly127 is hydrogen bonded to N1 of the adenine ring (distance = 2.95 Å) and AN7 of the adenine ring interacts with NH1 of Arg290 (NH1−AN7 distance = 4.12 Å), as in *C. fasciculata* and *T. cruzi* TRs. The ribose ring interacts mainly with Asp35 (distance OD1−AO2 = 2.71 Å; distance OD2−AO3 = 3.13 Å) as in the other TRs. Additionally, in *L. infantum* TR, AO3 is hydrogen bonded to the nitrogen atom of Ala47 (which substitutes Ser46 of *T. cruzi* TR). The pyrophosphate group is hydrogen bonded to the N and OG1 atoms of Thr51 (distances OA1−*N* = 2.89 Å, OA2−*N* = 3.35 Å; OA1−OG1 = 2.51 Å) and to the nitrogen of Ser14 (OP1−*N* = 3.40 Å, OA2−*N* = 3.23 Å). N of Asp327 is hydrogen bonded to O2P (distance = 3.15 Å). The ribosyl chain O3′ is hydrogen bonded to Asp327 (OD1−O3′ = 2.88, OD2−O3′ = 3.24 Å) and Leu334 (N−O3′ = 3.36 Å). Finally, the flavin ring interacts with the protein moiety by the O4 and N5 atoms hydrogen bonded to the NZ of Lys61 (NZ−O4 = 2.95 Å, NZ−N5 = 3.03 Å) (Figure 3B).

NADPH Binding Domain. The structure of reduced *L. infantum* TR in complex with Sb(III) and NADPH has been compared with the structure of *T. cruzi* TR in the reduced state, which was obtained in the presence of NADPH.[32] Unfortunately, the deposited PDB file of *T. cruzi* TR does not contain NADPH coordinates. However, the residues involved in NADPH binding[32] are almost completely conserved in the two proteins (Table 3 and Figure 4A). As shown in Figure 4A, the adenine moiety

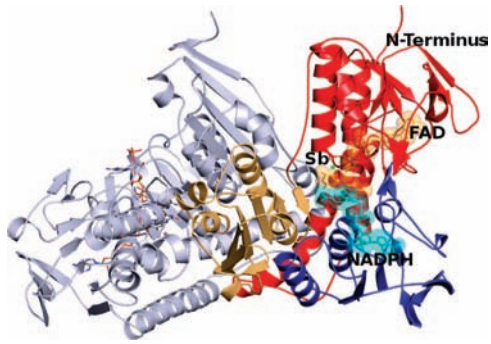

Figure 2. Overall fold of *L. infantum* TR in the oxidized form. One monomer of the dimer is colored gray. In the other monomer, the FAD binding domain (residues 1−160 and 291−360) is colored red, the NADPH binding domain (residues 161−290) blue, and the interface domain (361−488) in yellow-orange. The FAD and NADPH cofactors are indicated in stick, and Sb(III) is indicated as a green sphere. The figure was generated using PyMOL.[57]

Table 2. Spectroscopic, Physical, and Kinetic Parameters of *L. infantum* TR in Comparison with TR of *L. donovani* and *T. cruzi*[19]

	trypanothione reductase		
	L. infantum	*L. donovani*	*T. cruzi*
oligomeric structure	dimer	dimer	dimer
pyridine dinucleotide	NADPH	NADPH	NADPH
flavin	FAD	n.d.	FAD
K_m (μM) trypanothione disulfide	72 ± 9	36	45
K_m (μM) NADPH	12 ± 2.5	9	5
K_i (μM) for Sb(III)	1.5 ± 0.4	n.d.	n.d.
K_i (μM) for As(III)	14 ± 4	n.d.	n.d.
k_{cat} (min^{-1}) trypanothione disulfide	4800 ± 1100	10760	14200
k_{cat}/K_m (M^{-1} s^{-1})	1.1×10^6	5.0×10^6	5.3×10^6

does not interact directly with the protein, whereas the 2′-phosphate group is tightly bound, through its oxygen atoms, to Arg222, Arg228, and Tyr221. Tyr221 was expected to play a major role in the discrimination between NADH and NADPH in that, in human GR (which binds NADH), this residue is substituted by Ile217.[33] The pyrophosphate group is hydrogen bonded to Tyr198, which is phenylalanine in *T. cruzi* TR, and to the conserved Ile199 (see Table 3). Finally, the nicotinamide ribose interacts in both proteins with the conserved Met333, whereas the nicotinamide moiety interacts with both Glu202 and Ala365 (see Table 3 and Figure 4A).

The structures of oxidized TR and of reduced NADPH- and Sb(III)-bound TR are very similar, the superposition between the two structures yielding a rmsd of 0.378 Å. The most important differences are visible in the catalytic site and in the NADPH binding site (Figure 4B).

In the NADPH binding site, Arg222 and Tyr198 undergo conformational changes similar to those described for GRs.[34] The phenolic ring of Tyr198 is rotated by about 120° around the Cα−Cβ bond to accommodate the NADPH nicotinic ring, and Arg222 is rotated by about 30° around the Cα−Cβ bond to accommodate the adenine ring. Other small changes in the NADPH binding domain concern Arg228 and Tyr221, which interact with the adenine ribose phosphate in the reduced NADPH bound enzyme.

The residues interacting with the NADPH molecule are indicated in Figure 4B, and the distance between the NADPH atoms and the protein are shown in Table 3.

Catalytic Site and Sb(III) Binding Site. In the native TR structure, the two sulfur atoms of Cys52 and Cys57, are placed at a distance compatible with disulfide bond formation (2.05 Å), indicating that the native protein is completely oxidized (Figure 5A).

It is well-known that TR reduction is a prerequisite for Sb(III) binding.[19] For this reason, the TR complex with Sb(III) was

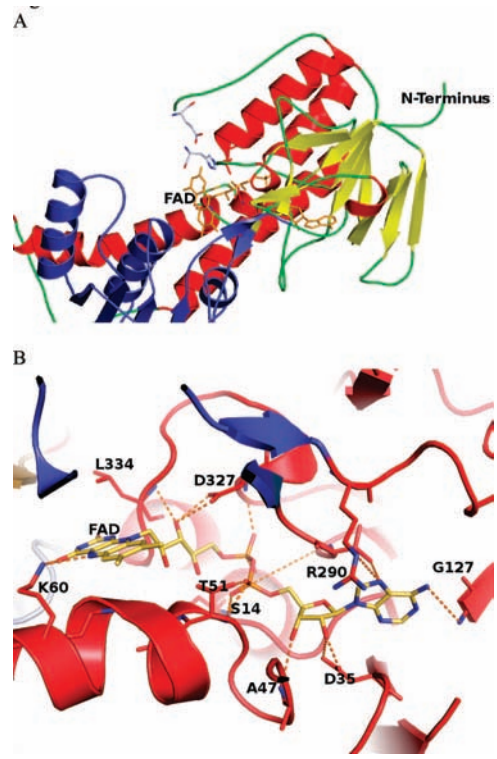

Figure 3. *L. infantum* TR FAD binding domain. (A) Overall view of the FAD binding domain displaying the typical Rossmann fold of GR family proteins. The α-helices are colored red, the β-strands and FAD yellow, the connecting loops green (blue helices belong to the NADPH-binding domain). (B) FAD binding site. The FAD molecule and the residues that interact with it are displayed. The picture was generated using PyMOL.[57]

Table 3. Residues within 3.5 Å Distance from NADPH in *Leishmania infantum* NADPH−Sb(III)−TR structure and in *T. cruzi* NADPH−TR structure

	T. cruzi TR		*L. infantum* TR	
atom of NADPH	atom (residue)	distance (Å)	atom (residue)	distance (Å)
	Adenine Ribose			
2′ phosphate O1	OH (Tyr221)	3.1	OH (Tyr221)	3.4
2′ phosphate O1	NH2 (Arg222)	2.6	NH2 (Arg222)	2.8
2′ phosphate O2	NH2 (Arg229)	2.9	NH1 (Arg228)	2.7
2′ phosphate O2	OH (Tyr222)	2.2	OH (Tyr221)	2.6
2′ phosphate O3	NH2 (Arg223)	3.1	NH2 (Arg222)	3.0
2′ phosphate O3	NH2 (Arg229)	2.7	NH1 (Arg228)	2.7
O3′	N (Gly197)	3.2		
	Pyrophosphate Group			
A-phosphate O1	N (Phe199)	3.5	N (Tyr198)	3.9
A-phosphate O2	N (Phe199)	2.9	N (Tyr198)	3.9
A-phosphate O2	N (Ile200)	2.9	N (Ile199)	3.0
	Nicotinamide Ribose			
O2′	O (Met333)	2.6	O (Met333)	2.9
	Nicotinamide			
O7	O (Ala365)	3.4	O (Ala365)	3.3
N7	OE2 (Glu203)	3.0	OE2 (Glu202)	3.2
N7	O (Ala365)	2.8	O (Ala365)	2.8
N7	O4α (flavin)	3.1	O4α (flavin)	3.3

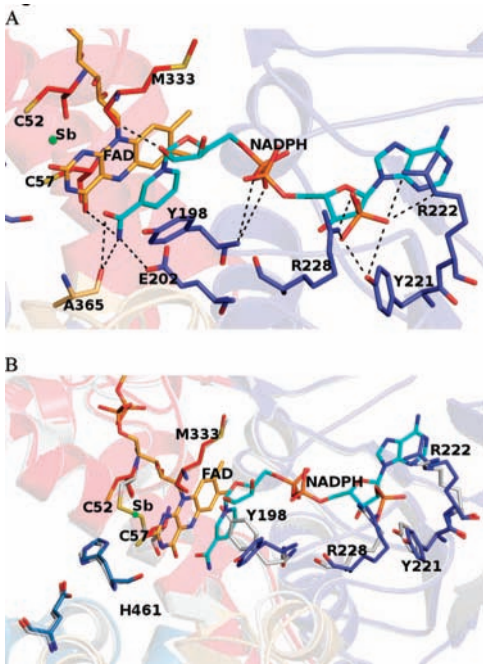

Figure 4. *L. infantum* NADPH binding site. (A) NADPH binding site in reduced TR in complex with Sb(III) and NADPH. The NADPH and FAD molecules, as well as the residues interacting with the NADPH, are indicated in sticks (the values of distances, indicated by dashed lines, are reported in Table 3). (B) Superposition between the NADPH domain of native oxidized TR (in gray) and the NADPH domain of the reduced TR in the complex. Secondary structure elements (light-shaded) and residues (sticks) belonging to the NADPH and FAD domain are colored blue and red, respectively. NADPH and FAD are colored cyan and yellow, respectively. Oxygen, nitrogen, sulfur, and antimony atoms are colored red, blue, yellow, and green, respectively.

obtained by soaking the TR oxidized crystals with a mother liquor solution containing 1 mM potassium antimonyl tartrate trihydrate and 5 mM NADPH.

The $F_o - F_c$ difference Fourier map shows a strong electron density peak (Figure 5B) that disappears only when the map is contoured at 7σ. This behavior clearly shows that the species present in that site has a number of electrons that is more than twice that of a water molecule and is compatible with a metal ion. Of all the ions present in the soaking solution, Sb(III) is both the only one present at high concentration and the only one that can be coordinated by cysteine residues.

Upon protein reduction, and Sb(III) binding the disulfide bridge breaks and the sulfur atoms move away to a distance of 4.4 Å (Figure 5C).

The antimony ion is bound in the catalytic cleft at the dimeric interface. Sb(III) is tetrahedrically coordinated by the two cysteines (SG Cys52−Sb(III) = 2.8 Å, SG Cys57−Sb(III) = 3.0 Å), one threonine residue (OG1 Thr335−SbIII = 3.0 Å), and His461′ of the 2-fold symmetry related subunit (ND1 His461′−Sb(III) = 3.2 Å) (Figure 5A). Moreover, the antimony trivalent ion is placed at a distance of about 4.49 and 4.33 Å from the FAD nitrogen atoms N5 and N10, respectively (Figure 5D).

To study the interaction of *L. infantum* TR with trypanothione, the structure of the protein in the reduced state has been superimposed to that of *T. cruzi* TR, which contains the trypanothione coordinates (PDB code: 1BZL). This comparative study shows that almost all *T. cruzi* residues that are involved in trypanothione binding are conserved in *L. infantum* TR. Assuming that the trypanothione mode of binding to *L. infantum* TR is not significantly different from that observed in the *T. cruzi* structure, trypanothione would interact with *L. infantum* TR Glu110, Tyr108, Glu18 on the FAD binding domain of one monomer and His461′ of the interface domain of the 2-fold symmetry related subunit, which is also a Sb(III) ligand. The residue homologous to His461′ in GRs (His467′ in human GR) is known to have an important role in the reduction mechanism of glutathione because it acts as a proton exchanger stabilized by the conserved Glu472′.[34] As shown in Figure 5D, His461′ is at hydrogen bond distance from the SG6 of the trypanothione molecule (NE2−SG6 = 2.87 Å) as well as from the SG of Cys52 (ND1−SG = 3.4 Å) and Cys57 (ND1−SG = 3.5 Å), which form the disulfide bridge in the oxidized protein. The analysis of the structure of the Sb(III)−TR complex clearly shows that trivalent antimony binding to the catalytic site interrupts the direct communication between His461′, the Cys residues, and the sulfur atoms of trypanothione, thus inhibiting TS_2 reduction.

Enzyme Assays and Enzyme Inhibition. Steady state condition kinetic experiments were carried out by varying the concentration of one of the two substrates (NADPH and TS_2) and keeping constant the concentration of the other (Table 2). After starting the reaction by the addition of TS_2, the absorbance decrease at 340 nm, which indicates the oxidation of NADPH (see Experimental Section), was measured.

The reaction catalyzed from *L. infantum* TR follows the Michaelis Menten equation with both NADPH and TS_2 substrates. The K_m values for NADPH is 12 μM, while it is 72 μM for TS_2. The k_{cat} is 4800 min^{-1} for trypanothione disulfide, which is 50−70% lower than that observed for other TRs.

The ability of Sb(III) and As(III) to inhibit TS_2 reduction catalyzed by TR was assessed. Different amounts of As_2O_3 and potassium antimonyl tartrate trihydrate have been added to a solution containing oxidized TR (see Experimental Section) and 200 μM NADPH. After starting the reaction by the addition of TS_2 at a concentration of 200 μM, the absorbance decreases at 340 nm, which indicates the oxidation of NADPH (see Experimental Section), was measured. The measured K_i for Sb(III) and As(III) are 1.5 ± 0.4 μM and 14 ± 4 μM, respectively, indicating that Sb(III) is a very effective inhibitor of the enzyme (Table 2).

Discussion

The trypanothione/TR system, which replaces the nearly ubiquitous glutathione/GR system, protects trypanosomatids from oxidative damage and toxic heavy metals and delivers the reducing equivalents for DNA synthesis. The known sensitivity of *Leishmania* parasites toward reactive oxygen species (ROS) and the absence of the trypanothione/TR system from the mammalian host make the enzymes of the trypanothione metabolism promising targets for the development of parasite-specific drugs. The work presented here shows that trivalent arsenicals and antimonials are able to bind with high affinity to the active site of *L. infantum* TR and inhibit its enzymatic activity. Most importantly, the structural analysis of TR in complex with Sb(III) and NADPH sheds light for the first time on the molecular mechanism of action of antimonial drugs.

TRs are members of the large and well-characterized family of FAD-dependent NAD(P)H oxidoreductases. These are dimeric flavoenzymes that catalyze the transfer of electrons between pyridine nucleotides and disulfide/dithiol compounds and promote catalysis via FAD and a redox active disulfide, such as GR, lipoamide dehydrogenase, and mercuric ion reductase.[35,36] TRs keep the main thiols of the *Leishmania* parasites, namely

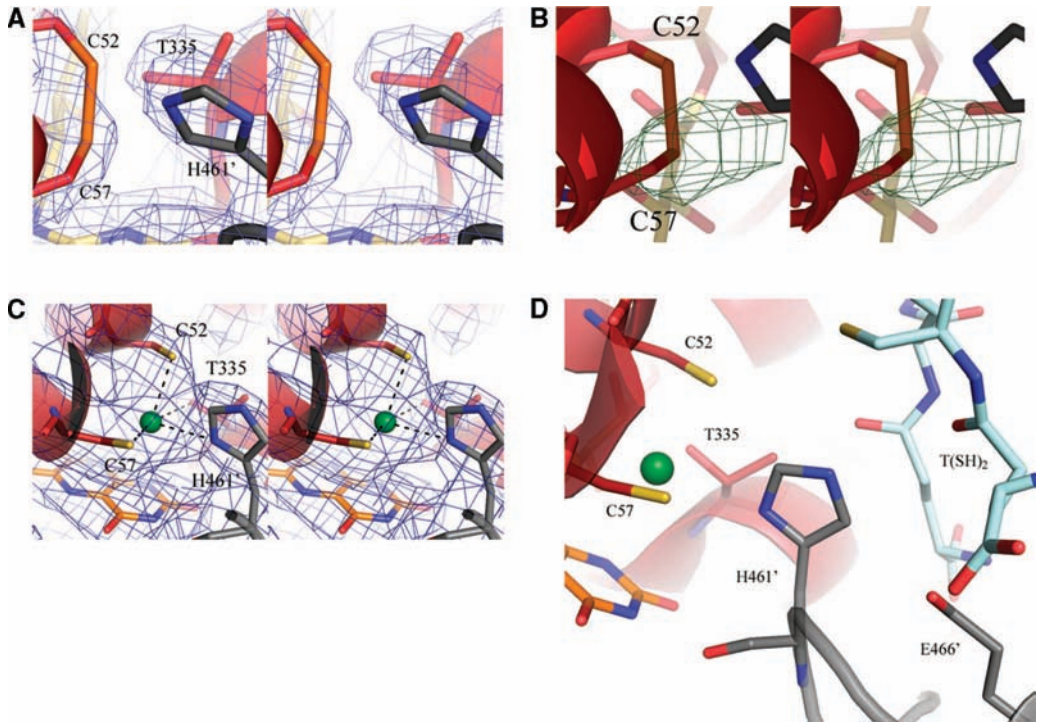

Figure 5. Catalytic site of TR from *Leishmania infantum*. (A) Stereo view of the catalytic site of oxidized TR and the corresponding electron density map $2F_o - F_c$ (in blue) contoured at 1σ. The residues (Cys52, Cys57, His461′, and Thr335) are indicated as sticks. Oxygen, nitrogen, and sulfur atoms are colored red, blue, and yellow, respectively. (B) Stereo view of the catalytic site of oxidized TR and the Fourier difference map $F_o - F_c$ (in green) contoured at 4σ. The F_o values were obtained from the experimental diffraction data collected for the reduced Sb(III)-bound TR crystal, and the F_c values were calculated from the oxidized TR structure. The residues forming the disulfur bridge (Cys52 and Cys57) are indicated as sticks. Oxygen, nitrogen, and sulfur atoms are colored red, blue, and yellow, respectively. (C) Stereo view of the Sb(III) binding site. The corresponding electron density map $2F_o - F_c$ (in blue) is contoured at 1σ. The Sb(III) coordinating residues (Cys52, Cys57, His461′, and Thr335) are indicated as sticks. Oxygen, nitrogen, sulfur, and antimony atoms are colored red, blue, yellow, and green, respectively. (D) Overall view of the catalytic cleft. The residues involved in trypanothione reduction are indicated as sticks. The trypanothione substrate, modeled on the basis of the *T. cruzi* TR structure (PDB code 1BZL), is also indicated as sticks and colored cyan.

monoglutathionylspermidine and bis(glutathionyl)spermidine [trypanothione, $T(SH)_2$] in the reduced state:

$$TS_2 + NADPH + H^+ \leftrightarrows T(SH)_2 + NADP^+$$

TRs share many physical and chemical properties with human GR, the closest related host enzyme, except their mutually exclusive specificity toward their disulfide-containing substrates.[37−39] Although not accepting glutathione as an alternate substrate, TRs resemble GRs in structure and mechanism of action.[34,40] The consensus mechanism for the reductase reaction begins with the binding of NADPH, which transiently reduces the flavin. Reduction of the cystine disulfide in the active site by the reduced flavin follows, by formation of a short-lived covalent intermediate with Cys57 and the subsequent formation of a stable charge-transfer complex between the flavin and the Cys57 thiolate. After formation of the charge-transfer complex, $NADP^+$ dissociates and is replaced by another NADPH. One of the protein cysteines, Cys52, which is activated similarly to serine and cysteine proteases by the His461′−Glu466′ pair (belonging to the second subunit of the dimer), can then react with TS_2 to produce a mixed disulfide followed by attack of the second protein cysteine (Cys57) on Cys52. This step releases the reduced $T(SH)_2$ and reforms the cystine disulfide in the enzyme.

Comparison of the residues interacting with NADPH in *L. infantum* and *T. cruzi* TR (Table 3) did not show any relevant change in distance and orientation, even considering the substitution of *L. infantum* Tyr198 with Phe198. However, in the structure of reduced TR in complex with Sb(III), the side chain of Tyr198 undergoes a 120° rotation with respect to oxidized TR, assuming a parallel conformation with the nicotinamide ring of NADPH (Figure 4B). In this way, stacking between the parallel rings of FAD, NADPH, and Tyr198 is formed that can establish $\pi-\pi$ interactions (distances between the rings around 4 Å).[41] Moreover, as in GRs and in the other proteins of the TR family, NADPH binding to *L. infantum* TR also promotes the displacement of residues interacting with the cofactor such as Arg228, Tyr221, and Arg222.[40]

Importantly, in *L. infantum*, TR the relative position of His461′, Glu466′ (which stabilizes the His positive charge during the redox reaction), Cys52, Cys57, and the docked trypanothione molecule is highly conserved with respect to *T. cruzi* TR. Additionally, as in the case of GRs, the position of these residues is identical in the oxidized and reduced states of the enzyme. Thus, it is clear that the mechanism of trypanothione reduction fits with the consensus scheme described for glutathione reduction by human GR.[34,42] The presence in the active site of His461′, which is fundamental for the catalysis and is provided by the 2-fold symmetry related subunit, explains why TR can be active only in the dimeric form.

TR is believed to be the in vivo target for arsenical and antimonial compounds, which exhibit antiparasitic activity. Further, $T(SH)_2$ may increase the activity of antimonials by promoting the reduction of Sb(V), although it might also promote parasite detoxification by forming a complex with Sb(III), subsequently extruded by an ATP-coupled efflux pump.[17,43,44] Pentavalent antimonials (Sb(V)), such as sodium stibogluconate (Pentostam) and meglumine antimonate (Glu-

cantime), have been the front-line drugs for more than half a century, although recently resistance against these drugs has been increasingly spreading.[8] Sb(V)-containing compounds are more effective and 10-fold less toxic than their trivalent analogues, although Sb(V) is considered to be a pro-drug that has to be activated by conversion to the trivalent form Sb(III)[18] to exert its action against the parasite. Reduction of Sb(V) may take place nonenzymatically by thiols[43] or be due to the parasite-specific enzyme, thiol-dependent reductase (TDR1)[45] and/or antimonite reductase (ACR2).[46] In particular, $T(SH)_2$ has been found to rapidly reduce Sb(V) to Sb(III), especially under acidic conditions and at slightly elevated temperature.[47] Reduction occurs preferentially in amastigotes, which have a lower intracellular pH and live at a higher temperature than promastigotes. Decreased levels of Sb(III) are observed in resistant strains with respect to the drug-sensitive strains due to inhibition of intracellular reductase activity or decreased uptake of Sb(III) caused by lower expression of the parasite aquaglyceroporin gene (AQP1), which is responsible for uptake of the metal.[48] Once the Sb(III) is in the cell and is conjugated to trypanothione, the complex can be sequestered inside a vacuole or extruded by ATP-binding cassette (ABC) transporters.[44,47,49]

Despite their long-standing clinical use, the mode of action of antimonials at a molecular level is poorly understood. Sb(III) was known to reversibly inhibit TR in vitro in two ways: by promoting loss of trypanothione and glutathione, thus decreasing intracellular thiol buffer capacity, and by increasing the intracellular concentration of the disulfide forms of these thiols through TR inhibition.[17,19] Sb(III) profoundly perturbs the thiol redox potential of the cell, thus exposing the parasites to oxidative damage caused by ROS produced by the host macrophages.[17]

The present study shows that TR from *L. infantum* is strongly inhibited by Sb(III) ions even at low concentrations. In fact, the measured K_i of 1.5 μM (Table 2) is indicative of a high affinity binding of Sb(III) to the protein. *L. infantum* TR is also inhibited, although at higher concentrations, by As(III), an ion with chemical and physical properties similar to those of Sb(III).

The structural analysis of the reduced TR in complex with NADPH and Sb(III) clearly shows for the first time that the trivalent ion binds in the catalytic cleft at the dimeric interface, engaging in complex formation the most important residues involved in trypanothione reduction, namely Cys52, Cys57, and His461′ of the 2-fold symmetry related subunit, thereby inhibiting the TR activity. Sb(III) is also coordinated to Thr335 (Figure 5C). Binding of the semimetal is only possible upon enzyme reduction because in the oxidized enzyme the two cysteine residues form a disulfur bridge.

Because Sb(III) has no role in either parasite or host metabolism, there are very few data on functional coordination of this semimetal in proteins. It is well-known that Sb(III) may coordinate up to six atoms (S, N, and/or O) in inorganic and organic complexes.[50] Thus, the trivalent antimonial ion may form complexes with different ligand geometries: it may coordinate three ligands and assume a planar coordination, four ligands with a tetrahedral coordination, and five or six ligands assuming a bipyramidal coordination with triangular or square base respectively. The only protein structure containing Sb(III) reported to date is the structure of the catalytic subunit of the *E. coli* ArsA ATPase.[20] The ArsAB pump, which consists of a soluble ATPase (ArsA) and a membrane channel (ArsB), provides resistance to both As(III) and Sb(III). The ATPase is activated upon binding of Sb(III) or As(III), the same ion(s) transported by the ArsAB pump. In this protein, a trinuclear Sb(III) cluster was found to be located at the interface between the two halves of the protein complex. Each of the three Sb(III) coordinates three donor atoms, two of which from protein residues of the two monomers and one from the Cl^- ion. The highest affinity Sb(III) ion is bound to two cysteine residues. Binding of Sb(III) or As(III) brings together the two domains of the enzyme.[20,51] The electron density map of the *L. infantum* Sb(III)−TR complex here reported clearly shows that Sb(III) is coordinated by Cys52, Cys57, His461′, and Thr335, with a coordination geometry that is a hybrid between a distorted tetrahedron and a trigonal bipyramid. This kind of coordination has been found in organic complexes as the tetra-*p*-tolyl-antimony nitrate, where the nitrate ion perturbs the coordination geometry of the tetra-*p*-tolyl-antimony.[52] In *L. infantum* TR−Sb(III) structure, the geometry of the complex may be modified by the π−cation interaction between Sb(III) and the FAD ring placed at a distance of about 4.0 Å from the Sb(III) ion. Finally, it should be mentioned that the ND1 nitrogen atom of His461′, which is directed toward Glu465′ in the TR protein family, coordinates the metal in the *L. infantum* TR−Sb(III) complex (the histidine ring is rotated of 180° around the Cβ carbon with respect to the oxidized form).

In conclusion, the present paper describes the first *Leishmania* TR structure and clearly demonstrates for the first time the mechanism of inhibition of the TR activity by Sb(III). The trivalent antimony, upon NADPH reduction of TR, binds to the protein with high affinity, thereby inhibiting the protein activity. The metal binds directly to Cys52, Cys57, Thr 335, and His461′ (belonging to the 2-fold symmetry related subunit), thereby disallowing the hydride transfer from the protein to the trypanothione and therefore trypanothione reduction. Such interaction is consistent with the modality of cysteine binding of thiophilic metals such as As(III), Sb(III), and Bi(III). Metal-bound cysteines are fully deprotonated thiolate anions, the nucleophilicity of which is greatly attenuated upon formation of metal complexes with high thermodynamic stability, which dissociate with very slow rates.[53,54] TR inhibition abolishes the main form of regulation of *Leishmania* cellular redox equilibrium and impairs the parasite's defense against oxidative stress by shifting the equilibrium toward the disulfide form of trypanothione, thereby perturbing the thiol redox potential of the cell.[17] We showed that the long-known antileishmanial action of antimonials is mainly due to their interaction with thiolate- and nitrogen-containing TR. TR is inhibited with high affinity by metals such as Sb(III) and As(III), which are drugs able to interact and inhibit thiol-dependent enzymes, and by palladium-containing compounds.[55] GRs, which have very similar structure and mechanism of action with respect to TRs, are also inhibited by many different metals. Such metal-dependent inhibition of thiol reductases opens the path to the possibility of a combined metal therapy of leishmaniasis.

Acknowledgment. This work was supported by the European Community−Research Infrastructure Action under the FP6 "Structuring the European Research Area" Programme (through the Integrated Infrastructure Initiative" Integrating Activity on Synchroton and Free Electron Laser Science, contract R II 3, CT-2004-506008). We thank Drs. Marina Gramiccia and Trentina Di Muccio for providing DNA and RNA samples of *L. infantum* and *L. major*, and Drs. Francesco Angelucci, Pierpaolo Ceci, and Veronica Morea for useful discussions. We thank the Berliner Elektronenspeicherring-Gesellschaft für Synchrotronstrahlung, BESSY (Berlin), where the data were col-

lected. FIRB 2003 "post-genomic structural biology: development of infrastructures for protein crystallography" and FIRB 2003 "enzymes and organometallic catalysers for sustainable chemistry" are also acknowledged.

References

(1) Alvar, J.; Yactayo, S.; Bern, C. Leishmaniasis and poverty. *Trends Parasitol.* **2006**, *22*, 552–557.
(2) Desjeux, P. The increase in risk factors for leishmaniasis worldwide. *Trans. R. Soc. Trop. Med. Hyg.* **2001**, *95*, 239–243.
(3) Croft, S. L.; Coombs, G. H. Leishmaniasis−current chemotherapy and recent advances in the search for novel drugs. *Trends Parasitol.* **2003**, *19*, 502–508.
(4) Desjeux, P. Leishmaniasis: current situation and new perspectives. *Comp. Immunol. Microbiol. Infect. Dis.* **2004**, *27*, 305–318.
(5) Murray, H. W.; Berman, J. D.; Davies, C. R.; Saravia, N. G. Advances in leishmaniasis. *Lancet* **2005**, *366*, 1561–1577.
(6) Sundar, S.; Benjamin, B. Diagnosis and treatment of Indian visceral leishmaniasis. *J. Assoc. Physicians India* **2003**, *51*, 195–201.
(7) Olliaro, P. L.; Guerin, P. J.; Gerstl, S.; Haaskjold, A. A.; Rottingen, J. A.; Sundar, S. Treatment options for visceral leishmaniasis: a systematic review of clinical studies done in India, 1980−2004. *Lancet Infect. Dis.* **2005**, *5*, 763–774.
(8) Croft, S. L.; Sundar, S.; Fairlamb, A. H. Drug resistance in leishmaniasis. *Clin. Microbiol. Rev.* **2006**, *19*, 111–126.
(9) Hunter, W. N.; Alphey, M. S.; Bond, C. S.; Schuttelkopf, A. W. Targeting metabolic pathways in microbial pathogens: oxidative stress and anti-folate drug resistance in trypanosomatids. *Biochem. Soc. Trans.* **2003**, *31*, 607–610.
(10) Krauth-Siegel, R. L.; Comini, M. A. Redox control in trypanosomatids, parasitic protozoa with trypanothione-based thiol metabolism. *Biochim. Biophys. Acta* **2008**, *1780*, 1236–1248.
(11) Linares, G. E.; Ravaschino, E. L.; Rodriguez, J. B. Progresses in the field of drug design to combat tropical protozoan parasitic diseases. *Curr. Med. Chem.* **2006**, *13*, 335–360.
(12) Dumas, C.; Ouellette, M.; Tovar, J.; Cunningham, M. L.; Fairlamb, A. H.; Tamar, S.; Olivier, M.; Papadopoulou, B. Disruption of the trypanothione reductase gene of Leishmania decreases its ability to survive oxidative stress in macrophages. *EMBO J.* **1997**, *16*, 2590–2598.
(13) Fairlamb, A. H.; Blackburn, P.; Ulrich, P.; Chait, B. T.; Cerami, A. Trypanothione: a novel bis(glutathionyl)spermidine cofactor for glutathione reductase in trypanosomatids. *Science* **1985**, *227*, 1485–1487.
(14) Flohe, L.; Hecht, H. J.; Steinert, P. Glutathione and trypanothione in parasitic hydroperoxide metabolism. *Free Radical Biol. Med.* **1999**, *27*, 966–984.
(15) Krieger, S.; Schwarz, W.; Ariyanayagam, M. R.; Fairlamb, A. H.; Krauth-Siegel, R. L.; Clayton, C. Trypanosomes lacking trypanothione reductase are avirulent and show increased sensitivity to oxidative stress. *Mol. Microbiol.* **2000**, *35*, 542–552.
(16) Tovar, J.; Wilkinson, S.; Mottram, J. C.; Fairlamb, A. H. Evidence that trypanothione reductase is an essential enzyme in Leishmania by targeted replacement of the tryA gene locus. *Mol. Microbiol.* **1998**, *29*, 653–660.
(17) Wyllie, S.; Cunningham, M. L.; Fairlamb, A. H. Dual action of antimonial drugs on thiol redox metabolism in the human pathogen *Leishmania donovani*. *J. Biol. Chem.* **2004**, *279*, 39925–39932.
(18) Goodwin, L. G.; Page, J. E. A study of the excretion of organic antimonials using a polarographic procedure. *Biochem. J.* **1943**, *37*, 198–209.
(19) Cunningham, M. L.; Fairlamb, A. H. Trypanothione reductase from *Leishmania donovani*. Purification, characterisation and inhibition by trivalent antimonials. *Eur. J. Biochem.* **1995**, *230*, 460–468.
(20) Zhou, T.; Radaev, S.; Rosen, B. P.; Gatti, D. L. Structure of the ArsA ATPase: the catalytic subunit of a heavy metal resistance pump. *EMBO J.* **2000**, *19*, 4838–4845.
(21) Baiocco, P.; Franceschini, S.; Ilari, A.; Colotti, G. Trypanothione reductase from *Leishmania infantum*: cloning, expression, purification, crystallization and preliminary X-ray data analysis *Protein Pept. Lett.* **2009**, *16*, 196−200.
(22) Otwinowski, Z.; Minor, W. Processing of X-ray Diffraction Data Collected in Oscillation Mode. *Methods Enzymol.* **1997**, *276*, 307–326.
(23) Vagin, A.; Teplyakov, A. MOLREP: an automated program for molecular replacement. *J. Appl. Crystallogr.* **1997**, *30*, 1022–1025.
(24) Murshudov, G. N.; Vagin, A. A.; Dodson, E. J. Refinement of macromolecular structures by the maximum-likelihood method. *Acta Crystallogr., Sect. D: Biol. Crystallogr.* **1997**, *53*, 240–255.
(25) Emsley, P.; Cowtan, K. Coot: model-building tools for molecular graphics. *Acta Crystallogr., Sect. D: Biol. Crystallogr.* **2004**, *60*, 2126–2132.
(26) Matthews, B. W. Solvent content of protein crystals. *J. Mol. Biol.* **1968**, *33*, 491–497.
(27) Zhang, Y.; Bond, C. S.; Bailey, S.; Cunningham, M. L.; Fairlamb, A. H.; Hunter, W. N. The crystal structure of trypanothione reductase from the human pathogen *Trypanosoma cruzi* at 2.3 A resolution. *Protein Sci.* **1996**, *5*, 52–61.
(28) Reynolds, C.; Damerell, C. J.; Jones S. ProtorP: a protein−protein interaction analysis tool *Bioinformatics* **2009**, *25*, 413−414.
(29) Bond, C. S.; Zhang, Y.; Berriman, M.; Cunningham, M. L.; Fairlamb, A. H.; Hunter, W. N. Crystal structure of *Trypanosoma cruzi* trypanothione reductase in complex with trypanothione, and the structure-based discovery of new natural product inhibitors. *Structure* **1999**, *7*, 81–89.
(30) Hunter, W. N.; Bailey, S.; Habash, J.; Harrop, S. J.; Helliwell, J. R.; Aboagye-Kwarteng, T.; Smith, K.; Fairlamb, A. H. Active site of trypanothione reductase. A target for rational drug design. *J. Mol. Biol.* **1992**, *227*, 322–33.
(31) Jacoby, E. M.; Schlichting, I.; Lantwin, C. B.; Kabsch, W.; Krauth-Siegel, R. L. Crystal structure of the *Trypanosoma cruzi* trypanothione reductase−mepacrine complex. *Proteins* **1996**, *24*, 73–80.
(32) Lantwin, C. B.; Schlichting, I.; Kabsch, W.; Pai, E. F.; Krauth-Siegel, R. L. The structure of *Trypanosoma cruzi* trypanothione reductase in the oxidized and NADPH reduced state. *Proteins* **1994**, *18*, 161–173.
(33) Karplus, P. A.; Pai, E. F.; Schulz, G. E. A. crystallographic study of the glutathione binding site of glutathione reductase at 0.3 nm resolution. *Eur. J. Biochem.* **1989**, *178*, 693–703.
(34) Karplus, P. A.; Schulz, G. E. Substrate binding and catalysis by glutathione reductase as derived from refined enzyme: substrate crystal structures at 2 Å resolution. *J. Mol. Biol.* **1989**, *210*, 163–180.
(35) Pai, E. F. Variations on a theme: the family of FAD-dependent NAD(P)H-(disulphide)-oxidoreductases. *Curr. Opin. Struct. Biol.* **1991**, *1*, 796–803.
(36) Williams, C. H. J. Lipoamide dehydrogenase, glutathione reductase, thioredoxin reductase, and mercuric ion reductase−A family of flavoenzyme transhydrogenases. In *Chemistry and Biochemistry of Flavoenzymes*; Müller, F. , Ed.; CRC Press: Boca Raton, FL, 1992; Vol. 3, pp 121−211.
(37) Bradley, M.; Bucheler, U. S.; Walsh, C. T. Redox enzyme engineering: conversion of human glutathione reductase into a trypanothione reductase. *Biochemistry* **1991**, *30*, 6124–6127.
(38) Shames, S. L.; Fairlamb, A. H.; Cerami, A.; Walsh, C. T. Purification and characterization of trypanothione reductase from *Crithidia fasciculata*, a newly discovered member of the family of disulfide-containing flavoprotein reductases. *Biochemistry* **1986**, *25*, 3519–3526.
(39) Shames, S. L.; Kimmel, B. E.; Peoples, O. P.; Agabian, N.; Walsh, C. T. Trypanothione reductase of *Trypanosoma congolense*: gene isolation, primary sequence determination, and comparison to glutathione reductase. *Biochemistry* **1988**, *27*, 5014–5019.
(40) Berkholz, D. S.; Faber, H. R.; Savvides, S. N.; Karplus, P. A. Catalytic cycle of human glutathione reductase near 1 A resolution. *J. Mol. Biol.* **2008**, *382*, 371–384.
(41) Chakrabarti, P.; Bhattacharyya, R. Geometry of nonbonded interactions involving planar groups in proteins. *Prog. Biophys. Mol. Biol.* **2007**, *95*, 83–137.
(42) Karplus, P. A.; Schulz, G. E. Refined structure of glutathione reductase at 1.54 Å resolution. *J. Mol. Biol.* **1987**, *195*, 701–729.
(43) Ferreira Cdos, S.; Martins, P. S.; Demicheli, C.; Brochu, C.; Ouellette, M.; Frezard, F. Thiol-induced reduction of antimony(V) into antimony(III): a comparative study with trypanothione, cysteinyl-glycine, cysteine, and glutathione. *Biometals* **2003**, *16*, 441–446.
(44) Mukhopadhyay, R.; Dey, S.; Xu, N.; Gage, D.; Lightbody, J.; Ouellette, M.; Rosen, B. P. Trypanothione overproduction and resistance to antimonials and arsenicals in Leishmania. *Proc. Natl. Acad. Sci. U.S.A.* **1996**, *93*, 10383–10387.
(45) Denton, H.; McGregor, J. C.; Coombs, G. H. Reduction of anti-leishmanial pentavalent antimonial drugs by a parasite-specific thiol-dependent reductase, TDR1. *Biochem. J.* **2004**, *381*, 405–412.
(46) Zhou, Y.; Messier, N.; Ouellette, M.; Rosen, B. P.; Mukhopadhyay, R. *Leishmania major* LmACR2 is a pentavalent antimony reductase that confers sensitivity to the drug pentostam. *J. Biol. Chem.* **2004**, *279*, 37445–37451.
(47) Yan, S.; Li, F.; Ding, K.; Sun, H. Reduction of pentavalent antimony by trypanothione and formation of a binary and ternary complex of antimony(III) and trypanothione. *J. Biol. Inorg. Chem.* **2003**, *8*, 689–697.
(48) Mittal, M. K.; Rai, S.; Ashutosh; Ravinder; Gupta, S.; Sundar, S.; Goyal, N. Characterization of natural antimony resistance in *Leishmania donovani* isolates. *Am. J. Trop. Med. Hyg.* **2007**, *76*, 681–688.

(49) Legare, D.; Richard, D.; Mukhopadhyay, R.; Stierhof, Y. D.; Rosen, B. P.; Haimeur, A.; Papadopoulou, B.; Ouellette, M. The Leishmania ATP-binding cassette protein PGPA is an intracellular metal-thiol transporter ATPase. *J. Biol. Chem.* **2001**, *276*, 26301–26307.
(50) Kasuga, N. C.; Onodera, K.; Nakano, S.; Hayashi, K.; Nomiya, K. Syntheses, crystal structures and antimicrobial activities of 6-coordinate antimony(III) complexes with tridentate 2-acetylpyridine thiosemicarbazone, bis(thiosemicarbazone) and semicarbazone ligands. *J. Inorg. Biochem.* **2006**, *100*, 1176–1186.
(51) Ruan, X.; Bhattacharjee, H.; Rosen, B. P. Cys-113 and Cys-422 form a high affinity metalloid binding site in the ArsA ATPase. *J. Biol. Chem.* **2006**, *281*, 9925–9934.
(52) Sharutin, V. V.; Sharutina, O. K.; Bondar′, E. A.; Pakusina, A. P.; Adonin, N. Y.; Starichenko, V. F.; Fukin, G. K.; Zakharov, L. N. Tetraphenylantimony Pentafluorobenzoate and tetra-*p*-Tolylantimony Nitrate: Syntheses and Structures. *Russ. J. Coord. Chem.* **2001**, *27*, 393–397.
(53) Chertova, E. N.; Kane, B. P.; McGrath, C.; Johnson, D. G.; Sowder, R. C., II; Arthur, L. O.; Henderson, L. E. Probing the topography of HIV-1 nucleocapsid protein with the alkylating agent *N*-ethylmaleimide. *Biochemistry* **1998**, *37*, 17890–17897.
(54) Apuy, J. L.; Busenlehner, L. S.; Russell, D. H.; Giedroc, D. P. Ratiometric pulsed alkylation mass spectrometry as a probe of thiolate reactivity in different metalloderivatives of *Staphylococcus aureus* pI258 CadC. *Biochemistry* **2004**, *43*, 3824–3834.
(55) Otero, L.; Vieites, M.; Boiani, L.; Denicola, A.; Rigol, C.; Opazo, L.; Olea-Azar, C.; Maya, J. D.; Morello, A.; Krauth-Siegel, R. L.; Piro, O. E.; Castellano, E.; Gonzalez, M.; Gambino, D.; Cerecetto, H. Novel antitrypanosomal agents based on palladium nitrofurylthiosemicarbazone complexes: DNA and redox metabolism as potential therapeutic targets. *J. Med. Chem.* **2006**, *49*, 3322–3331.
(56) Thompson, J. D.; Higgins, D. G.; Gibson, T. J. CLUSTAL W: improving the sensitivity of progressive multiple sequence alignment through sequence weighting, position-specific gap penalties and weight matrix choice. *Nucleic Acids Res.* **1994**, *22*, 4673–4680.
(57) DeLano, W. L. *The PyMOL Molecular Graphics System*; DeLano Scientific: San Carlos, CA, 2002.

JM900185Q